Biomass Conversion and Biorefinery (2024) 14:20883–20896
https://doi.org/10.1007/s13399-023-04443-y

ORIGINAL ARTICLE

Investigation of the Remazol Turquoise GN dye adsorption using silane-modified silica prepared from agricultural waste

Mujgan Okur[1] · **Dilsad Dolunay Eslek Koyuncu**[1]

Received: 27 January 2023 / Revised: 31 May 2023 / Accepted: 1 June 2023 / Published online: 27 June 2023

Abstract

In this study, silica sorbents obtained from paddy waste ash were functionalized with (3-Aminopropyl) trimethoxysilane (APTMS) and 3-Glycidyloxypropyl) trimethoxysilane (GPTMS), and used in the adsorption of Remazol Turquoise GN (RTGN) dye in a batch system. The effects of pH (2–8) and the concentration of dye (20–100 mg/L) on the dye removal were investigated. To explain the adsorption mechanism, Langmuir, Freundlich, Temkin and Henry adsorption isotherm models were used. The Langmuir model for Si-APTMS and the Henry model for Si-GPTMS were found to be in agreement with the experimental data. Pseudo first and second-order kinetic models were used for the investigating the adsorption kinetics. It was seen that the adsorption process with Si-APTMS and Si-GPTMS was expressed by Pseudo second-order kinetic model. The dye removal capacities of these sorbents were obtained as 273.87 and 27.51 mg/g, respectively. The dye adsorption behavior of the modified silica sorbents was confirmed by Thermogravimetric (TG), Fourier-transform infrared spectroscopy (FT-IR) and X-ray photoelectron spectroscopy (XPS) analyzes. The higher dye removal ability of Si-APTMS sorbent was correlated with the amine functionality of this sorbent. According to the analysis results and proposed adsorption mechanism, it was determined that the electrostatic interaction between the charged $-NH_3^+$ in the sorbent surface and the $-SO_3^-$ groups in anionic dye molecule was mainly responsible for the adsorption process.

Keywords Paddy waste ash · GPTMS · APTMS · Remazol dye · Adsorption kinetics

1 Introduction

The textile, paper, paint, printing, plastic, iron-steel, and medicine industries use large amounts of water and organic-based compounds [1, 2]. In particular, textile, paint, and paper industries frequently use synthetic dyes. Because of not using these dyes effectively, about 5–10% of them are mixed with wastewater [3, 4]. Unfortunately, this value reaches around 50% in reactive dyes [5].

Membrane filtration, flocculation, ion exchange, electrocoagulation, ozonation, adsorption, biodegradation, and photocatalytic degradation are widely known methods for dye removal. Most of these methods are low-efficiency and costly techniques [6-8]. It should be noted that the choice of method depends on several factors such as the type and concentration of dye, water quality, and treatment requirements. Researchers continue to explore new materials and technologies to increase dye removal efficiency, reduce operating and production costs, and minimize environmental impact. Among these methods, adsorption is preferred due to its advantages [9]. The application of adsorption is relatively simple. It can be applied in batch systems or continuous flow systems, depending on the scale and requirements of the application. It does not require complex equipment or complex process control. Many adsorbents can be regenerated and reused many times. This makes adsorption a cost-effective and sustainable method for dye removal. In addition, adsorption is a flexible technique and can be combined with other techniques. It can act as a pretreatment step to reduce the dye concentration before further processing. Recently, biomass-derived carbon materials [10], graphene oxide-based aerogels [11], magnetized materials [12], mesoporous silica [13], amino-functionalized silica [14], and cellulose aerogel [15] have attracted attention in the dye adsorption studies. Researchers are constantly researching and developing

✉ Mujgan Okur
mtelli@gazi.edu.tr

[1] Department of Chemical Engineering, Gazi University, 06570 Ankara, Turkey

new adsorbents with improved properties for better dye removal. In recent years, the use of agricultural wastes in the production of high-value-added products such as adsorbents has become increasingly important. In the study of Cimirro et al. [16], *Pinus elliottii* sawdust, an abundant sawmill residue, was utilized as a carbon source to prepare activated biochar at 600 °C. The prepared sample was investigated for the removal of catechol (CAT), resorcinol (RES), and hydroquinone (HYD) diphenols. According to Liu isotherm model, the highest adsorption capacity was 419.8 (CAT at 45 °C), 263.8 (RES 40 °C), and 500.9 mg/g (HYD 25 °C). The prepared carbon was also tested for simulated industrial waste, and removal of up to 95.97% was achieved. In another study, Reis et al. [17] activated Norway spruce bark with $MgCl_2$, $ZnSO_4$, $ZnCl_2$, and KOH agents, and tested them for acetaminophen adsorption. Guy et al. [18] investigated the activation parameters of Norway spruce bark with KOH. The prepared sorbent was used to remove the Evans blue dye and cyclic tests showed that this sorbent could be regenerated efficiently. Sun et al. [10] prepared corncob porous carbon (CPC) by a simple carbonization-activation procedure. Activation was carried out at 600, 700, 800, 900, or 1000 °C for 0.5, 1, 2, or 3 h using KOH. The prepared carbon samples were tested for supercapacitor and dye adsorption. They mentioned that CPC showed high adsorption capacity (249.06 mg/g) and removal rate (99.87%) for Rhodamine B dye adsorption. Salomon et al. [19] utilized Pacara Earpod tree and Ironwood seeds to prepare low-cost biosorbents for the adsorption of basic fuchsin. Banerjee and Chattopadhyaya [20] investigated the removal of tartrazine, an anionic dye, using sorbents prepared from agricultural by-product sawdust. Materials obtained from paddy residues are frequently preferred in dye adsorption due to their high surface area, low cost, and easy preparation steps. In the literature, studies on the removal of different dyes by using sorbents derived from paddy husk have been found. Costa and Paranhos [21] used the paddy husks and ash obtained by burning paddy husks for the removal of Remazol Red dye. Tabassam et al. [22] modified the biochar obtained from paddy husks with cinnamic acid. They stated that carboxylic groups were added to the structure with cinnamic acid modification and thus the adsorption of methylene blue, a cationic dye, was more effective. In another study, Haider et al. [23] investigated the adsorption of methylene blue with silica materials obtained from paddy husks and stated that the adsorption capacity of this silica was 107 mg dye/g sorbent. Kaykioglu and Gunes [24] prepared magnetic nanoparticles using paddy husk ash burned at 300 °C. They concluded that this material could be used as a low-cost adsorbent to remove Acid Red 114 dye. Homagai et al. [25] studied the removal of Crystal Violet dye with carbonized paddy husk (CRH) and xanthate paddy husk (XRH) prepared from paddy husks. They carried out experiments on the adsorbent amount, concentration, pH, and contact time parameters and determined the most appropriate pH value as 10. They stated that equilibrium was reached in about 60 min. The adsorption capacities of CRH and XRH materials were found to be 62.85 and 90.02 mg/g, respectively. In another study, Quansah et al. [26], investigated the adsorption of methylene blue and Crystal Violet cationic dyes. In the study of Quansah et al., thermal treatment was applied to paddy husks at different temperatures (75, 100, 300, 500, and 700 °C) and their adsorption behavior was tested. They stated that paddy husks thermally treated at 75 °C exhibit higher adsorption capacity than adsorbents treated at 300–700 °C. They emphasized that in the paddy husks processed at high temperatures, the surface melts, and a cristobalite structure is formed due to the high silica content, which results in the clogging of the pores. In our previous study [27], paddy waste ash (PA) was utilized for producing carbon–silica hybrid (PCS) and silica (PS) aerogels. Prepared sorbents were tested for the removal of RTGN dye from wastewater. The adsorption capacities of PCS and PS were found to be 26.0 and 1.4 mg/g, respectively.

It is possible to improve the adsorption behavior of sorbents by surface modification. Kani et al. [28] prepared polyethyleneimine (PEI)-modified tiger nut using glutaraldehyde as a crosslinking agent to improve the sorbent behavior toward Congo red anionic dye. The maximum adsorption capacity of the sorbent was found to be 274 mg/g at 30 °C. In another study, Lee et al. [29] modified the mesoporous silica with APTMS using the post-synthesis grafting method. They determined that the increase in APTMS concentration was inversely proportional to the surface area but directly proportional to the Cr(VI) removal. Cavalcante et al. [30] prepared amino silica-functionalized biomass using 3-Aminopropyltriethoxysilane (APTES) and a tannin-rich grape residue for the removal of Methyl Orange.

High surface area silica aerogels have a pearl-necklace-like skeletal structure [31]. Despite their strong skeleton structure, weak interparticle bonds cause these materials to have low mechanical strength. There are various methods to improve the mechanical properties of these materials. Some of these methods are prolonging the aging time, increasing the number of surface crosslinks with a polymer, adding a second component before gelation, and using different silica sources in the silica skeleton [32]. Silica aerogel production studies have focused on the use of different silica sources or modification of synthesis parameters. It is possible to use biomass residues as a green and inexpensive source

of silica. Among the biomass residues, paddy waste has a high silica content. It is stated that the ash obtained when the paddy wastes are burned contains approximately 96% silica. Silica aerogel materials can be prepared by leaching this silica with NaOH as a sodium silicate solution (Eq. 1) [33].

$$xSiO_2 + 2NaOH \rightarrow Na_2O.xSiO_2 + H_2O \quad (1)$$

In the second step of the synthesis, silica aerogel structure begins to form at pH ≤ 10 in the presence of an acidic environment such as HCl (Eq. 2).

$$Na_2O.xSiO_2 + 2HCl \overset{pH\leq 10}{\rightarrow} xSiO_2 + 2NaCl + H_2O \quad (2)$$

At this stage, the removal of the formed NaCl salt is important for the formation of the silica aerogel structure. In literature studies, it has been reported that ion exchange resins can be used for this purpose [34]. However, the fact that this method requires the regeneration of the resin makes it difficult to apply in terms of time and cost. For this reason, washing with deionized water has been preferred in recent studies [35]. A few studies focus on the usage of silica aerogel prepared from paddy waste in dye adsorption in the literature. Shaban et al., (2017) [7] prepared MCM-48-supported nickel oxide-containing sorbents from silica aerogel obtained from paddy husks and used it for Congo Red removal. Hasanin, 2020 [36] prepared a hybrid material by mixing silica aerogel obtained from paddy husks with a polyvinyl alcohol binder. This hybrid material was functionalized using nicotinic acid and used in the adsorption of Methyl Orange and Methylene Blue. In another study, silica aerogel prepared from paddy husk ashes was modified with APTES and used in Methylene Blue adsorption [37]. In our previous study [38], APTMS and GPTMS-modified silica samples prepared from paddy waste ash were tested for cationic dye Rhodamine-B adsorption, and low adsorption capacities were observed (6.24 and 12.38 mg/g, respectively). The APTMS and GPTMS-modified silica aerogel sorbents have not been used before for the adsorption of RTGN metal complex dye.

The main concept of this work was the improvement of the adsorptive properties of silica recovered from paddy waste by applying modification with APTMS and GPTMS. As can be seen in the literature survey, APTMS and GPTMS-modified silica aerogel sorbents have not been used for the adsorption of RTGN metal complex dye. In this study, APTMS and GPTMS-modified silica aerogel samples prepared from the paddy waste ash were used as sorbents in the adsorption of RTGN dye. Removal of pollutant dye through the evaluation of agricultural waste doubles the environmental contribution of the study. The effects of modifying agent, pH, and initial dye concentration on the properties and sorbent behavior of the silica aerogel samples were examined. Langmuir, Freundlich, Temkin, and Henry isotherm models were used to investigate the adsorption mechanism. To examine the dye adsorption kinetics, Pseudo first-order and second-order kinetic models were applied. Dye adsorption behavior of the sorbents was confirmed by ATR/FT-IR, XPS and TG analysis.

2 Experimental

2.1 Preparation of Modified Silica Aerogel Materials

In this study, modified silica aerogels were prepared from the evaluation of paddy waste ash as a silica source. Paddy waste ash was provided by a company that burns paddy waste for power generation. The synthesis procedure mainly consists of silica extraction from ash, gelation and aging by solvent exchange, silane modification, and drying steps.

In the synthesis, 200 mL of 2 M NaOH solution was first added to 10 g of paddy waste ash, and stirring was continued for 2 h at 100 °C. At this stage, amorphous silica was extracted from the paddy waste ash, and sodium silicate was obtained as the liquid phase. The liquid phase was then separated by vacuum filtration, and neutralized by adding 2 M HCl (until pH 7). Then, the aging of the obtained gel was carried out by keeping it at room temperature for 20 h. The solid precipitate was recovered by vacuum filtration, rinsed with deionized water several times, and placed in an ethanol medium for solvent exchange. The solvent exchange was performed every 24 h for a week. The modification step was conducted at the final step of the solvent exchange by mixing the silica suspension with an ethanolic solution of the modifying agent (10% v/v). After modification with organosilane structures (3-Aminopropyl) trimethoxysilane-APTMS and 3-Glycidyloxypropyl) trimethoxysilane-GPTMS), freeze drying was applied to obtain modified silica aerogel materials. The silica aerogel samples prepared using this procedure were named Si-APTMS and Si-GPTMS, respectively.

2.2 Characterization of the sorbents

The effects of modification and dye adsorption on the physicochemical properties of the sorbents were investigated by Fourier-transform infrared spectroscopy (FT-IR), X-ray photoelectron spectroscopy (XPS), and Thermogravimetric Analysis (TGA). The structural bonds and functional groups after modification and dye adsorption were evaluated by FT-IR analysis performed in a Jasco 4700 ATR/FT-IR spectrophotometer in the medium infrared region (between 4000 and 400 cm^{-1}) with a

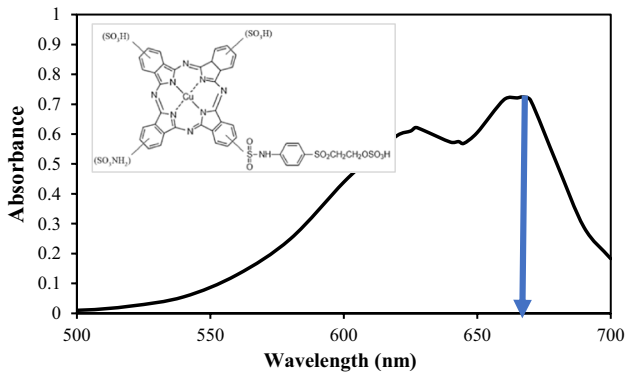

Fig. 1 The chemical structure and UV spectra of the RTGN dye

high resolution of 4 cm^{-1}. The surface chemistry of the samples was analyzed by XPS analysis performed in a SPECS EA300 instrument. TG analysis was carried out in an air atmosphere (45 mL/min), at a heating rate of 10 °C/min and in the temperature range between 30 and 800 °C using a Setaram Labsys Thermogravimetry Analysis and Differential Thermal Analysis System. N_2 adsorption–desorption analyses were conducted at 77 K using Quantachrome Autosorb-1C equipment, and the multipoint surface areas of the samples were calculated using Brunauer–Emmett–Teller (BET) method.

2.3 Adsorption Experiments

The sorbent behavior of the prepared samples was investigated in the batch adsorption process using the RTGN dye (Fig. 1). In the dye adsorption experiments, the effect of initial pH (2–8) and adsorption time were investigated at 30 °C with dye concentrations between 20 and 100 mg/L, 1 g/L sorbent and 100 rpm shaking speed in a batch system. In dye removal experiments, samples were taken from the dye solution at certain time intervals, and the dye concentration was analyzed using a PG Instruments T80 + Double Beam UV spectrometer at 667 nm wavelength (Fig. 1) at pre-determined time intervals.

The dye removal percentage and capacity (q) were calculated using Eq. 3 and 4 [39].

$$Dye\ removal\ percentage = \frac{(C_o - C_t)}{C_o} * 100 \quad (3)$$

$$Adsorption\ capacity, q_t = \frac{(C_o - C_t) * V}{m} \quad (4)$$

In these equations; C_o (mg/L) is the dye concentration at time t = 0, C_t (mg/L) is the dye concentration in the medium at time t, V (L) is the volume of the dye solution, m (g) is the amount of Si-APTMS and Si-GPTMS sorbents, and q_t (mg/g) is the amount of RTGN dye onto Si-APTMS and Si-GPTMS at time t.

3 Results and Discussion

3.1 Effect of pH on dye adsorption

In this study, Si-APTMS and Si-GPTMS sorbents prepared using the sol–gel method were evaluated in the adsorption of RTGN dye. First, the effect of pH on dye adsorption was examined in the range of 2–8 (Fig. 2). It is seen that the highest dye adsorption was obtained at pH 2 for both sorbents. At pH 2, the dye removal percentages were found to be 100% and 25.1% for Si-APTMS and Si-GPTMS, respectively. As the pH increased from 2 to 8, the percentages of dye removal decreased for both sorbents. This is due to the anionic character of the dye. It was reported that the effect of pH value on the adsorption behavior can be expressed by the isoelectric point of the sorbent surface [20]. The isoelectric point is the pH at which the zeta potential of the surface takes a zero value. At pH values lower than the isoelectric point, the surface of the sorbent is protonated, thereby increasing the electrostatic interaction between the anionic dye and the sorbent surface. As a result, the adsorption of the anionic dye increases [40]. In this study, consistent results were observed with the RTGN dye and silica aerogel sorbents. In our previous study, the zeta potentials for APTMS and GPTMS-modified silica samples were measured in the pH range of 2–12, and the isoelectric points of the sorbents were determined as 5.2 and 4.2, respectively [38]. In this study, it was seen that the dye removal percentages obtained at the pH values lower than the isoelectric points became higher. Besides, the dye removal percentages decreased at the pH values above the isoelectric points.

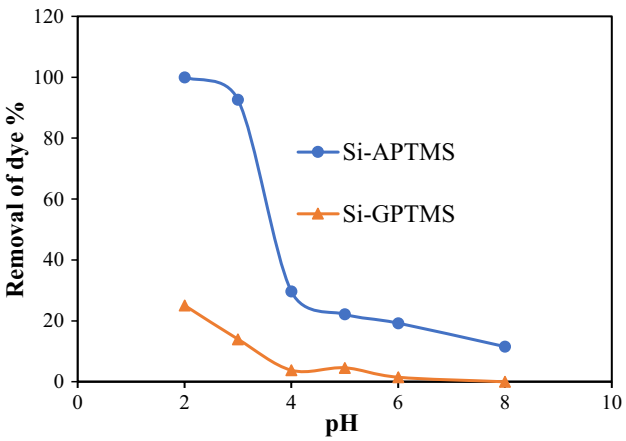

Fig. 2 The effect of pH on the dye removal percentage

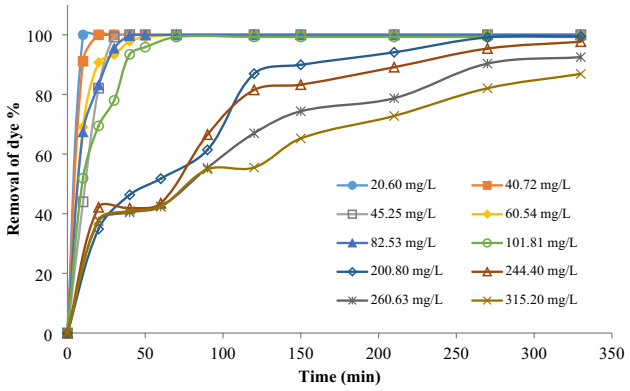

Fig. 3 Dye removal percentages of Si-APTMS (at pH = 2)

3.2 Effect of dye concentration on dye adsorption

The effect of dye concentration on the RTGN dye removal was investigated at pH 2 where the highest dye removal was achieved and in the concentration range of 20.60–315.20 mg/L for Si-APTMS and 20.60–101.81 mg/L for Si-GPTMS (Fig. 3 and 4). In adsorption experiments, it can be said that dye adsorption with Si-APTMS and Si-GPTMS is a fast process. In the adsorption experiments with Si-APTMS, the adsorption process was completed in the first 20 min at low dye concentrations (20.60 and 40.72 mg/L). At the dye concentrations of 45.25 mg/L and above, the adsorption reached equilibrium at the 40th minute. At dye concentrations of 200.80–315.20 mg/L, the time for the adsorption to reach equilibrium is more than 330 min. In the experiments conducted with Si-APTMS sorbent, it was observed that all dye in the medium was adsorbed at the dye concentration range being studied (20.60–101.81 mg/L). In the range of 200.77–315.20 dye concentrations, 87–99.5% dye removal was obtained. In the experiments with Si-GPTMS, the adsorption process was completed in the first 10 min at low dye concentrations (20.60 and 40.72 mg/L). At dye concentrations of 45.25 mg/L and above, the adsorption process was completed in 30 min. In the studied dye concentration range, 20.63–273.87 mg/g with Si-APTMS and 12.67–27.51 mg/g with Si-GPTMS were obtained. In the study of Eslek Koyuncu and Okur (2021), the adsorption capacity obtained with unmodified silica is 1.4 mg/g [27]. Lee et al. [29] investigated chromium removal with APTMS functionalized mesoporous silica in their study and 36.95–83.50 mg/g chromium removal was obtained. Donia et al. [41] performed acid dye adsorption with Amine modified silica and stated that the adsorption increased due to the interaction between amine groups on the adsorbent surface and sulfonate groups ($-SO_3^-$) of the dye.

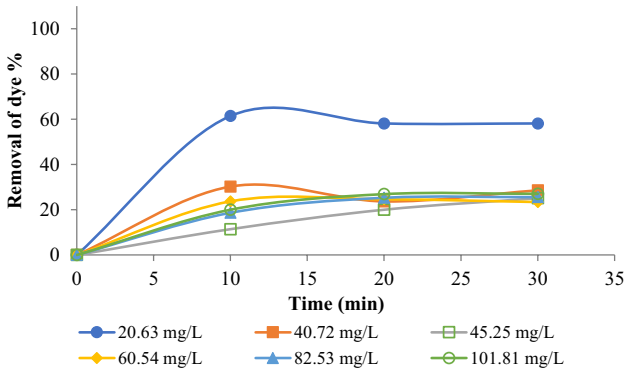

Fig. 4 Dye removal percentages of Si-GPTMS (at pH = 2)

3.3 Adsorption Isotherms

Adsorption isotherm equations were used to investigate the dye adsorption mechanism. For this purpose; Langmuir, Freundlich, Temkin, and Henry adsorption isotherm models were used, and the linear forms of these models are given by the following equations [42]:

$$\text{Langmuir Model } \frac{C_e}{q_e} = \frac{1}{q_m K_L} + \frac{C_e}{q_m} \tag{5}$$

$$\textit{Freundlich Model } lnq_e = lnK_F + \left(\frac{1}{n}\right) lnC_e \tag{6}$$

$$\text{Temkin Model } q_e = q_T(lnK_T + lnC_e) \tag{7}$$

$$\text{Henry Model } q_e = K_H C_e \tag{8}$$

In these equations; q_e, the equilibrium dye amount adsorbed onto the sorbent (mg/g); Ce, the equilibrium dye concentration (mg/L); q_m, the monolayer adsorption capacity (mg/g); K_L, the Langmuir constant (L/g) and related to the free energy of adsorption [43]. In addition, K_L is the Freundlich constant ((mg/g)(L/mg)$^{1/n}$), n is the Freundlich adsorption intensity, K_T is the Temkin constant (L/mg), q_T is the differential surface capacity for dye adsorption per unit binding energy, and K_H is the Henry isotherm constant. The Langmuir adsorption isotherm model is used to express monolayer adsorption on homogeneous surfaces. The Freundlich isotherm model represents to explain the multilayer isotherm on heterogeneous surfaces. The Temkin isotherm model is used to explain the interaction between adsorbate molecules adsorbed on the adsorbent surface [42]. The linear forms of these adsorption isotherm models were applied to experimental adsorption data for both sorbents. The adsorption

Table 1 Adsorption isotherm model constants

Model	Parameters	Si-APTMS	Si-GPTMS
Langmuir	q_m (mg/g)	270.3	37.04
	K_L (L/mg)	2.47	0.0206
	R^2	0.996	0.500
Freundlich	*1/n*	0.078	0.316
	K_F ((mg/g)(L/mg)$^{1/n}$)	200.66	5.14
	R^2	0.914	0.478
Temkin	q_T (mg/g)	21.11	5.68
	K_T	12.23	0.537
	R^2	0.978	0.468
Henry	K_H (mg/g)	9.06	0.24
	R^2	0.879	0.776

isotherm model constants obtained from these adsorption equations were calculated and given in Table 1. Additionally, the adsorption capacity (qe_{exp}) values obtained from the adsorption experiments performed with Si-APTMS and Si-GPTMS and the adsorption capacity (qe_{model}) values obtained from the adsorption isotherm model equations are given comparatively in Figs. 5 and 6. Langmuir, Freundlich, Temkin, and Henry adsorption isotherm models applied to the experimental data were compared in terms of correlation coefficients (R^2). The Langmuir model for Si-APTMS and the Henry model for Si-GPTMS was found to agree with the experimental data. In the Freundlich model, the 1/n value was found to be 0.078 for Si-APTMS. A value of 1/n between 0 and 1 indicates that the adsorption occurs on heterogeneous surfaces.

Additionally, the R_L values were calculated for Si-APTMS and Si-GPTMS. R_L is the dimensionless separation factor, and it shows whether the adsorption process is

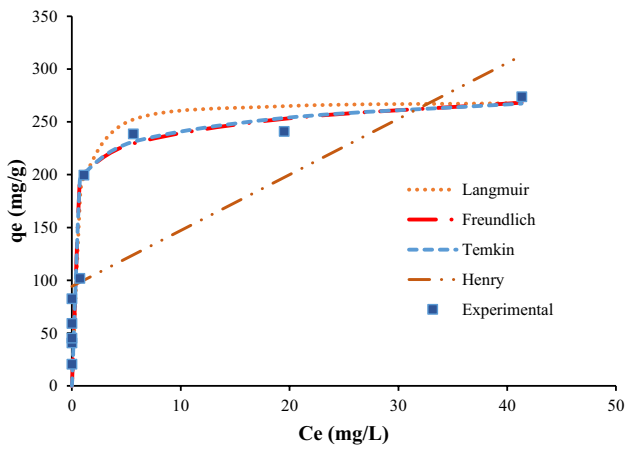

Fig. 5 Comparison of adsorption isotherm models for Si-APTMS

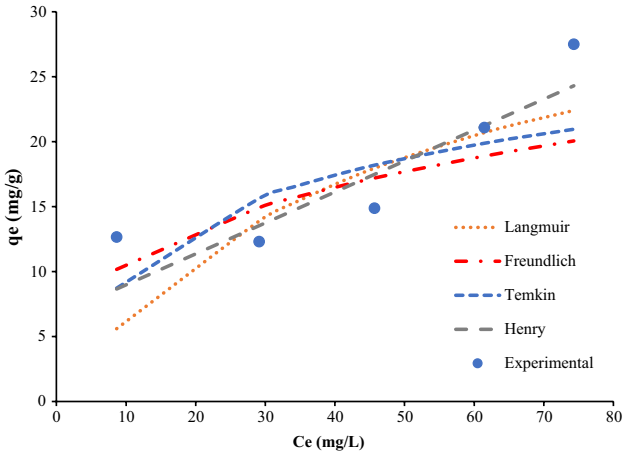

Fig. 6 Comparison of adsorption isotherm models for Si-GPTMS

favorable or unfavorable. R_L value was calculated using the formula given below [27];

$$R_L = \frac{1}{1 + K_L C_o} \tag{9}$$

where K_L is the Langmuir constant, and C_o is the initial dye concentration (mg/L). The values of R_L between 0 and 1 indicate that the adsorption is favorable. The values of $R_L > 1$, $R_L = 1$, and $R_L = 0$ indicate that the adsorption is unfavorable, linear, and irreversible, respectively [39]. In this study, the R_L values were found between 0.0193 and 0.0013 for Si-APTMS, and 0.323–0.7 for Si-GPTMS. These results revealed that the adsorption process of dye was favorable.

3.4 Adsorption Kinetics

Pseudo first-order (Eq. 10) and second-order (Eq. 11) kinetic models were used to examine the dye adsorption kinetics with Si-APTMS and Si-GPTMS. The linearized versions of these equations are given below [44]:

$$\text{Pseudo} - \text{first order } \ln\left(q_e - q_t\right) = \ln q_e - k_1 t \tag{10}$$

$$\text{Pseudo} - \text{second order } \frac{t}{q_t} = \frac{1}{k_2 q_e^2} + \frac{t}{q_e} \tag{11}$$

Here, k_1 and k_2 are the pseudo first-order and pseudo second-order adsorption rate constants, q_e and q_t are the dye amount adsorbed onto the sorbent at equilibrium and at time t (mg/g), respectively. Pseudo first-order and second-order kinetic model equations were applied to the experimental data and the parameters were calculated (Table 2).

When the pseudo first-order and pseudo second-order kinetic models were compared in terms of R^2 values, it was

Table 2 Pseudo first-order and second-order kinetic constants of Si-APTMS and Si-GPTMS

	C_o (mg/L)	qe_{exp} (mg/g)	Pseudo first-order			Pseudo second-order		
			qe_{mod} (mg/g)	k_1 (min^{-1})	R^2	qe_{mod} (mg/g)	k_2 (min^{-1})	R^2
Si-APTMS	20.63	20.63	0.006	0.127	0.331	20.62	$3.91*10^{12}$	1.000
	40.72	40.72	2.22	0.119	0.575	40.98	0.0735	0.999
	45.25	45.25	64.03	0.189	0.843	49.75	0.0034	0.964
	60.54	60.54	83.6	0.119	0.948	62.50	0.0065	0.996
	82.53	82.53	387.40	0.194	0.920	87.72	0.0028	0.989
	101.81	101.09	317.10	0.125	0.818	108.70	0.0013	0.972
	200.77	199.68	260.68	0.019	0.926	227.27	0.000099	0.965
	244.34	238.71	228.01	0.013	0.971	263.16	0.000084	0.957
	260.63	241.13	245.13	0.012	0.919	270.30	0.000071	0.952
	315.20	273.87	238.27	0.009	0.947	294.12	0.000071	0.951
Si-GPTMS	20.63	12.67	0.25	0.011	0.001	11.93	0.392	0.999
	40.72	12.31	0.61	0.016	0.003	11.11	0.488	0.977
	45.25	11.36	40.85	0.262	0.755	12.20	0.014	0.821
	60.54	14.89	3.11	0.142	0.273	14.28	0.471	0.999
	82.53	21.09	44.12	0.289	0.956	21.83	0.029	0.980
	101.81	27.51	47.63	0.281	0.970	28.49	0.024	0.982

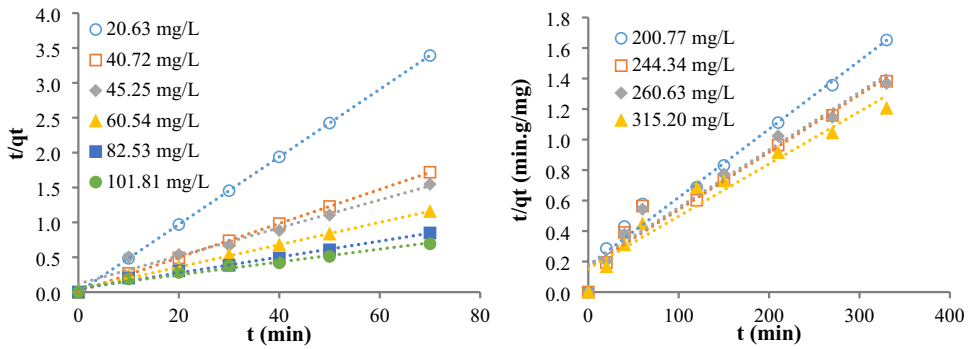

Fig. 7 Pseudo second-order kinetic model for Si-APTMS

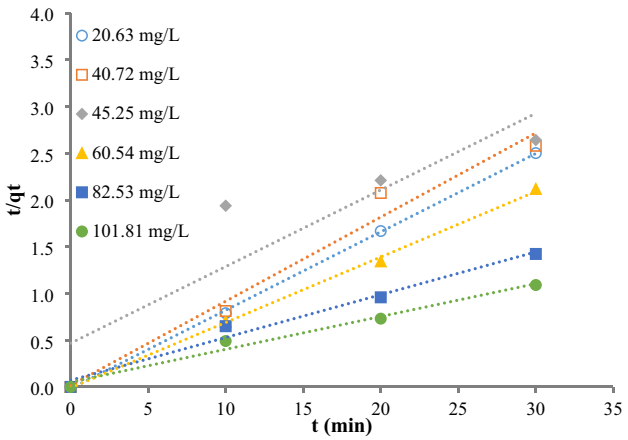

Fig. 8 Pseudo second-order kinetic model for Si-GPTMS

seen that the adsorption data obtained using Si-APTMS and Si-GPTMS did not fit well with the pseudo first-order kinetic model. However, the pseudo second-order kinetic model was found to be in good agreement with the experimental data (Fig. 7 and 8). It was observed that the R^2 values obtained from the pseudo second-order model were higher than the R^2 values obtained from the pseudo first-order kinetic model. In the literature studies on the Methylene Blue adsorption with porous silica [45], the organic dye adsorption with amino silica spherical particles [46], and the anionic dye adsorption with cationic-modified silica gel [47] the pseudo second-order kinetic model well described the adsorption kinetics.

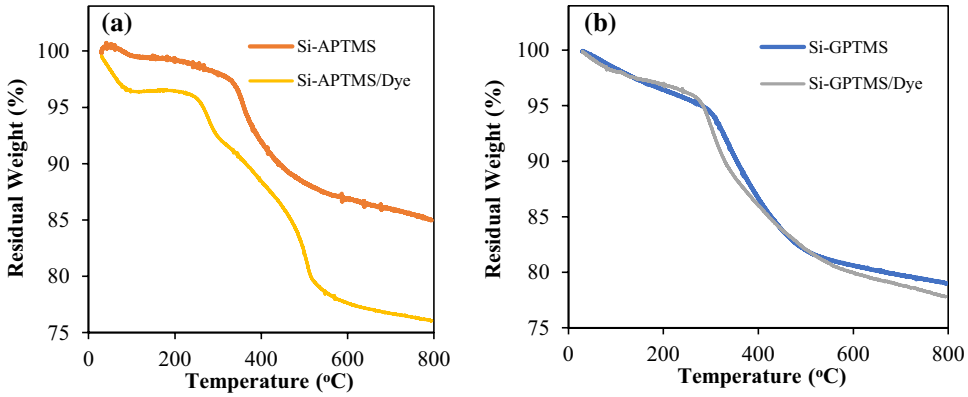

Fig. 9 TGA curves of **(a)** Si-APTMS and **(b)** Si-GPTMS samples before and after dye adsorption

3.5 Characterization Studies Before and After Dye Removal

In this study, ATR/FT-IR, XPS, and TG analyses were performed to determine the dye adsorption and to compare the dye adsorption behavior of the sorbents. These analyses were applied to the samples before and after dye adsorption. Firstly, the TGA was applied to the Si-APTMS and Si-GPTMS samples (Fig. 9). The weight losses in the Si-APTMS sample were considered in two stages. Due to the low boiling point of APTMS (< 95 °C), the weight losses observed around 30–200 °C were attributed to the removal of molecular water and physically adsorbed APTMS from the silica surface. The main decomposition of chemically bound APTMS was observed between 300 and 500 °C as reported in the literature [48]. From the TG analysis, it was determined that most of the APTMS were bound chemically. It is seen that the TGA curves of the Si-APTMS and Si-APTMS/Dye are different. The difference between the total weight loss of Si-APTMS and Si-APTMS/Dye was associated with the thermal degradation of dye adsorbed on the sorbent surface. For better comparison, the total weight change observed in the samples was calculated using the following equation:

$$\Delta m(\%) = \frac{m_{30} - m_{800}}{m_{30}} x100 \quad (12)$$

where m_{30} and m_{800} are the initial weight percentage and the remaining weight percentage of the sample at 800 °C in the TG analysis, respectively. The total weight loss of Si-APTMS and Si-APTMS/Dye samples was calculated as 15% and 24%, respectively. The difference between the total weight change of unused and used

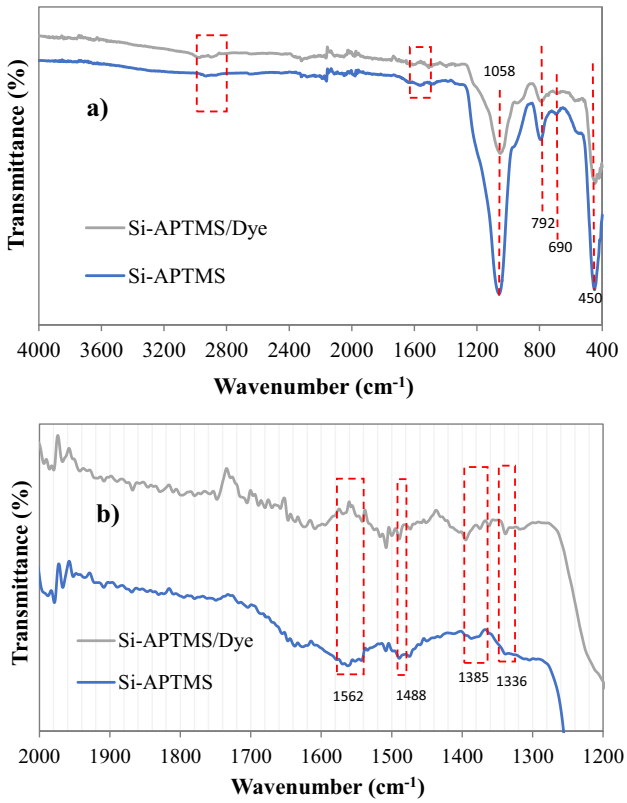

Fig. 10 ATR/FT-IR spectra of Si-APTMS sorbent before and after dye adsorption **(a)** 4000–400 cm^{-1} region, **(b)** 2000–1200 cm^{-1} region

Si-APTMS samples was found as about 9%. It was determined that this difference was related to the adsorbed dye amount on this sample. This value was about 1.3% for the Si-GPTMS sample. These results confirmed the previously mentioned higher experimental dye adsorption capacity of the Si-APTMS sorbent. The fact that

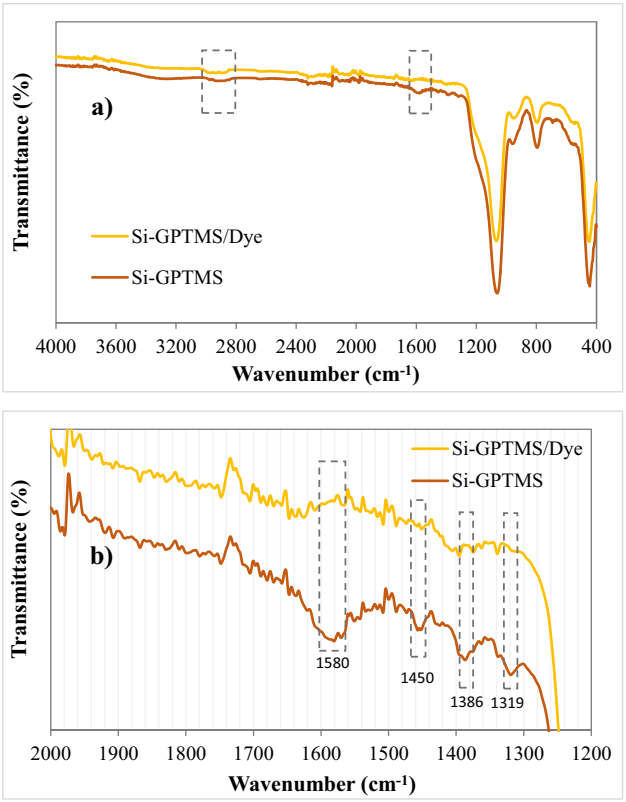

Fig. 11 ATR/FT-IR spectra of Si-GPTMS sorbent before and after dye adsorption **(a)** 4000–400 cm^{-1} region, **(b)** 2000–1200 cm^{-1} region

the TGA curves of the Si-GPTMS and Si-GPTMS/Dye samples were very close to each other suggested that the adsorption was physical.

The structural and functional groups present in the sorbent structure were determined by ATR/FT-IR analyses before and after dye adsorption. The characteristics of ATR measurements were observed between 1900 and 2400 cm^{-1} as small vibrations as shown in Figs. 10 and 11. It is seen that all samples exhibited bands around 450 cm^{-1}, 792 cm^{-1} and 1058 cm^{-1}. The peaks around 1058 cm^{-1} and 792 cm^{-1} were related to the asymmetric and symmetrical stretching of the Si–O-Si (siloxane). The peak at 450 cm^{-1} corresponded to the bending vibrations of siloxane.

In the ATR/FT-IR spectra of the Si-APTMS sample, the peaks at 2868 and 2932 cm^{-1} were attributed to the stretching vibration of C-H bonds [49]. In the dye-loaded Si-APTMS sample (Si-APTMS/Dye), the intensity of these peaks slightly increased due to adsorbed dye onto the sorbent. To clearly understand the structural and functional changes after dye adsorption, 1200–2000 cm^{-1} region of

Table 3 Atomic Si, O, N, and C concentrations in the samples

Sample	Si	O	N	C
Unmodified silica	25.4	72.9	< 0.1	1.6
Si-APTMS	23.7	57.9	3.6	14.7
Si-APTMS/Dye	22.1	52.4	4.2	21.3

the ATR/FT-IR spectra is given as a second Fig. (Fig. 10-b). The peak at 1562 cm^{-1} in the Si-APTMS sample was related to the bending vibration of the N–H bond of the APTMS structure. These results confirmed that the modification of the silica aerogel with APTMS was successfully performed [50]. It is seen that this peak disappeared in the Si-APTMS/Dye due to the interaction between the dye and NH_2 groups of the APTMS agent. Additionally, the peaks at 1336, 1385, and 1488 cm^{-1} were attributed to the presence of CH_2 (-C-H) groups of APTMS in the Si-APTMS sample. The intensities of these peaks did not change after the dye adsorption.

Figure 11 exhibits the ATR/FT-IR spectra of the Si-GPTMS sample before and after dye adsorption. The stretching and bending vibrations of Si-CH_2 in the Si-GPTMS were observed at 2960 and 1386 cm^{-1} [50]. The presence of these peaks was attributed to the successful modification of the silica structure with GPTMS. Additionally, the peaks at 1319 and 1450 cm^{-1} were attributed to the presence of CH_3 groups of GPTMS in the Si-GPTMS sample. A slight decrease in the intensity of the CH_3 groups can be attributed to the hydrolysis of GPTMS with water under an acidic medium [51, 52].

Small vibrations at 1562 cm^{-1} in the Si-APTMS and 1580 cm^{-1} in the Si-GPTMS sample were attributed to the skeletal C = C bond. These vibrations were not observed in the dye-loaded samples. Tran et al., (2017) [53] stated that the absence of these vibrations after dye adsorption related to the contribution of π- π interaction in the dye adsorption. In this study, it was thought that the adsorption process might be related to the π-π interaction in addition to the electrostatic interaction. As mentioned previously, higher dye removal was obtained with Si-APTMS than with Si-GPTMS. It was thought that the higher dye removal by Si-APTMS was due to the presence of amine groups in the structure of Si-APTMS.

In our previous study, unmodified silica sorbent was prepared from paddy waste ash, and it was seen that the point of zero charge of the sorbent was lower than 2. This sorbent exhibited the highest removal capacity of 61% at pH 2. It has been reported in the literature that the addition of amine functionality to the silica structure increases the zero charge point [54] as seen in this study. The increase in

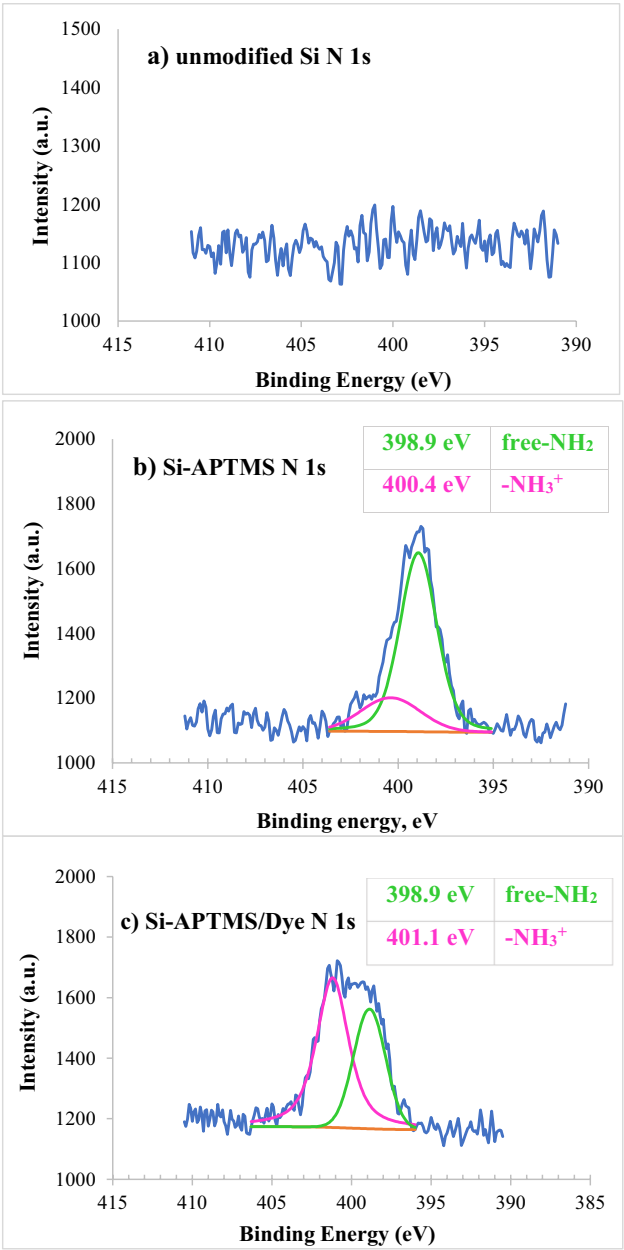

Fig. 12 Deconvoluted N 1s XPS peaks for **(a)** unmodified silica, **(b)** Si-APTMS and **(c)** Si-APTMS/Dye samples

the zero charge point was considered an important parameter for large-scale industrial applications and especially for anionic dyes.

In this study, the XPS technique was used to investigate the chemical composition and chemical bonding after modification with APTMS and dye adsorption due to its high adsorption property. The Si, O, N, and C concentrations determined by XPS analysis are presented in Table 3. The presence of N and C atoms in the unmodified silica sample was attributed to the contaminant of organic impurities [55]. The increase in the percentage of N and C in the Si-APTMS sample confirmed the modification of the silica surface by APTMS. Additionally, the increased amounts of N and C in the Si-APTMS/Dye sample indicated dye adsorption onto the Si-APTMS surface.

The deconvoluted high-resolution N 1s XPS spectra of the unmodified, APTMS-modified, and used silica sorbents are displayed in Fig. 12. It was reported that in the APTMS-modified samples, the high-resolution N 1s spectrum consists of two different peaks corresponding to free-NH_2 (398.8 eV) and -NH_3^+ (401.3 eV) [29, 56]. In this study, it is seen in Fig. 12-a that N 1s signals are absent in the unmodified silica sample as expected [55]. In the N 1s spectrum of the modified silica sample, free-NH_2 and -NH_3^+ peaks were observed around 398.9 eV and 400.4 eV, respectively (Fig. 12-b). This result supported the modification of the silica surface by APTMS [29]. Kani et al. determined that the ionic forces between the charged NH_3^+ and the anionic dye are responsible for the high adsorption capacity of the amine-modified sorbents [28]. The dye-adsorbed sample Si-APTMS/Dye exhibited a higher -NH_3^+ peak than Si-APTMS. It was thought that the increase in the intensity of the -NH_3^+ peak after dye adsorption was due to the low pH value of the adsorption solution, that is, the high H^+ ion concentration (Fig. 12-c).

3.6 Proposed Adsorption Mechanism for RTGN by Si-APTMS

In this study, the ATR/FT-IR and XPS analysis results confirmed the -NH_2 modification of the silica surface with APTMS and dye adsorption. Figure 13 depicts the proposed silica aerogel modification and adsorption mechanism for the RTGN dye onto Si-APTMS. In the aqueous phase modification of the silica surface with APTMS, the first hydrolysis occurs and then hydrolyzed APTMS reacts with the silica surface in different configurations including monodentate, bidentate, and tridentate (Fig. 13-a). In the acidic adsorption environment, -NH_2 groups were protonated to form -NH_3^+ on the surface. According to the analysis results and proposed adsorption mechanism (Fig. 13-b), it was determined that the electrostatic interaction between the charged -NH_3^+ and the -SO_3^- groups in the anionic dye molecule was mainly responsible for the adsorption process. Moreover, hydrogen bonding might be present between the free-NH_2/-OH^- groups of the sorbent and -SO_3^- groups in the dye molecule.

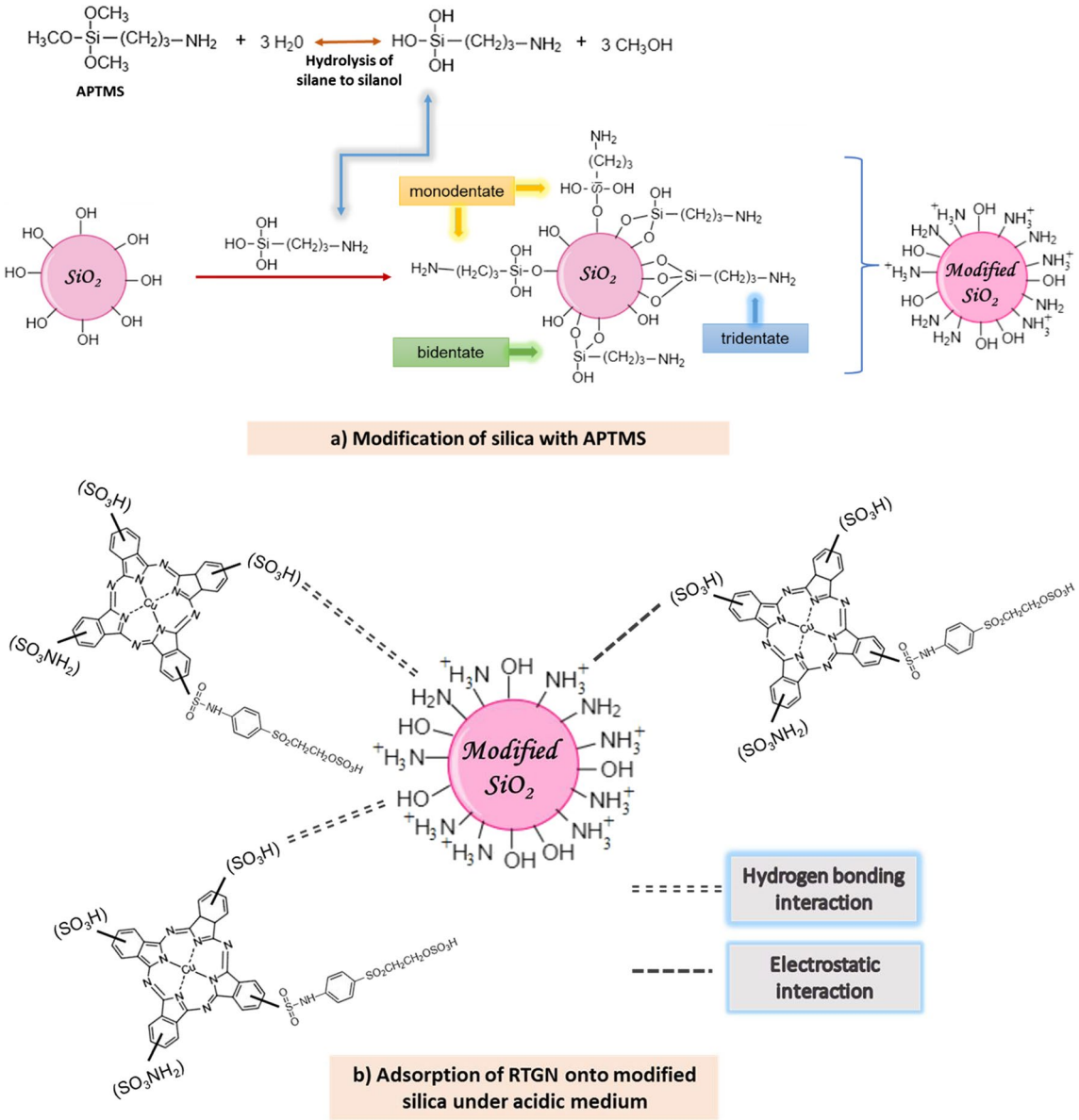

Fig. 13 Silica modification and proposed adsorption mechanism for RTGN dye adsorption onto Si-APTMS sorbent

4 Conclusion

The main concept of this study was the improvement of the adsorptive properties of silica recovered from paddy waste by applying modification with APTMS and GPTMS. Table 4 includes the adsorption results of the different sorbents reported in the literature. In our previously published study [27], unmodified silica sorbent exhibited low adsorption capacity (1.40 mg/g) in RTGN adsorption. In our preliminary experiments [38], APTMS and GPTMS-modified silica sorbents were tested for cationic Rhodamine-B adsorption, and low adsorption capacity values were obtained. In this study, RTGN dye adsorption performances of the Si-APTMS and Si-GPTMS were investigated. In adsorption experiments, the structural (pore volume, surface area, etc.) and surface properties of the sorbent are important parameters that affect the dye adsorption behavior of the sorbent. The specific surface area of Si-APTMS and Si-GPTMS sorbents were found as 415

Table 4 Adsorption capacities of the different silica sorbents

Adsorbent	Adsorbate	q (mg/g)	References
APTMS functionalized mesoporous silica	Chromium	36.95–83.50	[29]
Soy protein acid hydrolysate/silica hybrid material	Methylene blue	357	[57]
Silica aerogel	Basic dye	24.60–39.76	[43]
Silica/ZSM-5	Methylene blue	303	[45]
Ionic liquid modified silica nanoparticles	Anionic organic dyes	243.67	[58]
Amino silica	Organic dyes	55–262	[46]
Amine modified silica	Acid dyes	15.50–58.10	[41]
vinyl hybrid silica	Methylene blue	1609	[59]
nanocrystalline ZSM-5	Cationic dye	125.43	[2]
Silica aerogel/polyacrylonitrile/polyvinylidene fluoride nanofiber	Basic Red 18	188.70	[60]
Unmodified-silica	RTGN	1.40	[27]
Si-APTMS	RTGN	273.87	This study
Si-GPTMS	RTGN	27.51	This study

and 408 m^2/g, respectively. The pore volume values of these materials were also found to be quite close (2.25 cm^3/g for Si-APTMS and 2.70 cm^3/g for Si-GPTMS) [38]. However, it was observed that the dye removal percentages of APTMS and GPTMS-modified silica sorbents were different due to different surface properties. Functional amine groups are present in the APTMS structure and these groups played an important role in the dye adsorption process. According to the XPS analysis results, it was observed that electrostatic interaction and hydrogen bonds were effective between the amine groups in the Si-APTMS structure and the $-SO_3^-$ groups in the dye molecule. However, it was thought that the π-π interaction mechanism might play a role in addition to the electrostatic interaction in dye adsorption with Si-GPTMS. As a result, higher dye removal was obtained with Si-APTMS than with Si-GPTMS since Si-APTMS contains amine groups in its structure. At the end of the application of the adsorption isotherm models to the experimental data, it was found that the Langmuir model for Si-APTMS and the Henry model for Si-GPTMS were compatible with the experimental data. Here it can be said that the adsorption process occurs on single-layered homogeneous surfaces. Additionally, it was observed that the adsorption processes with Si-APTMS and Si-GPTMS were expressed by the pseudo second-order kinetic model. As a result, the adsorption capacities obtained from the adsorption of the dye with Si-APTMS and Si-GPTMS were obtained as 101.09 and 27.51 mg/g, respectively. This study showed that the adsorption capacity of silica can be highly improved by the modification with APTMS and GPTMS for the adsorption of RTGN dye. It was thought that this improvement was related to the increase in zeta-potential of the sorbent surface. As a result, it was concluded that GPTMS and APTMS-modified silica sorbents can be used successfully in dye adsorption.

Acknowledgements This work was supported by the Scientific Research Projects Coordination Unit of Gazi University under Grant Number # 06/2020-05. The authors thank to the Central Laboratory of METU for the characterization results.

Author contribution *Müjgan Okur:* Conceptualization; Data curation; Formal analysis; Investigation; Methodology; Roles/Writing—original draft; Writing—review & editing.

Dilşad Dolunay Eslek Koyuncu: Conceptualization; Data curation; Formal analysis; Funding acquisition; Investigation; Methodology; Roles/Writing—original draft; Writing—review & editing.

Data availability Not applicable.

Code availability Not applicable.

Declarations

Ethics approval Not applicable.

Conflict of interest The authors declare no competing interests.

Consent to participate Not applicable.

Consent for publication All authors agreed to publication.

References

1. da Rocha HD, Reis ES, Ratkovski GP et al (2020) Use of PMMA/(rice husk ash)/polypyrrole membranes for the removal of dyes

and heavy metal ions. J Taiwan Inst Chem Eng 110:8–20. https://doi.org/10.1016/j.jtice.2020.03.003
2. Sivalingam S, Sen S (2020) Rice husk ash derived nanocrystalline ZSM-5 for highly efficient removal of a toxic textile dye. J Market Res 9:14853–14864. https://doi.org/10.1016/j.jmrt.2020.10.074
3. Arora S, Saini HS, Singh K (2005) Decolorisation of a monoazo disperse dye with Candida tropicalis. Color Technol 121:298–303
4. Rai HS, Bhattacharyya MS, Singh J et al (2005) Removal of dyes from the effluent of textile and dyestuff manufacturing industry: A review of emerging techniques with reference to biological treatment. Crit Rev Environ Sci Technol 35:219–238. https://doi.org/10.1080/10643380590917932
5. Ertuğrul S, San NO, Dönmez G (2009) Treatment of dye (Remazol Blue) and heavy metals using yeast cells with the purpose of managing polluted textile wastewaters. Ecol Eng 35:128–134. https://doi.org/10.1016/j.ecoleng.2008.09.015
6. Safa Y, Bhatti HN (2011) Biosorption of Direct Red-31 and Direct Orange-26 dyes by rice husk: Application of factorial design analysis. Chem Eng Res Des 89:2566–2574. https://doi.org/10.1016/j.cherd.2011.06.003
7. Shaban M, Abukhadra MR, Hamd A et al (2017) Photocatalytic removal of Congo red dye using MCM-48/Ni2O3 composite synthesized based on silica gel extracted from rice husk ash; fabrication and application. J Environ Manage 204:189–199. https://doi.org/10.1016/j.jenvman.2017.08.048
8. Zhu H, Jiang R, Li J et al (2017) Magnetically recyclable Fe3O4/Bi2S3 microspheres for effective removal of Congo red dye by simultaneous adsorption and photocatalytic regeneration. Sep Purif Technol 179:184–193. https://doi.org/10.1016/j.seppur.2016.12.051
9. Domingues JT, Orlando RM, Sinisterra RD et al (2020) Polymer-bixin nanofibers: A promising environmentally friendly material for the removal of dyes from water. Separation and Purification Technology 248:117118. https://doi.org/10.1016/j.seppur.2020.117118
10. Sun Z, Qu K, Li J et al (2021) Self-template biomass-derived nitrogen and oxygen co-doped porous carbon for symmetrical supercapacitor and dye adsorption. Adv Composites Hybrid Mater 4:1413–1424. https://doi.org/10.1007/s42114-021-00352-8
11. Han M, Xu B, Zhang M et al (2021) Preparation of biologically reduced graphene oxide-based aerogel and its application in dye adsorption. Sci Total Environ 783:147028. https://doi.org/10.1016/j.scitotenv.2021.147028
12. Al-Musawi TJ, Mengelizadeh N, Al Rawi O, Balarak D (2022) Capacity and Modeling of Acid Blue 113 Dye Adsorption onto Chitosan Magnetized by Fe2O3 Nanoparticles. J Polym Environ 30:344–359. https://doi.org/10.1007/s10924-021-02200-8
13. Boukoussa B, Mokhtar A, El Guerdaoui A et al (2021) Adsorption behavior of cationic dye on mesoporous silica SBA-15 carried by calcium alginate beads: Experimental and molecular dynamics study. J Mole Liquids 333:115976. https://doi.org/10.1016/j.molliq.2021.115976
14. Cao Y, Malekshah RE, Heidari Z et al (2021) Molecular dynamic simulations and quantum chemical calculations of adsorption process using amino-functionalized silica. J Mole Liquids 330:115544. https://doi.org/10.1016/j.molliq.2021.115544
15. Huang C, Cai B, Zhang L et al (2021) Preparation of iron-based metal-organic framework @cellulose aerogel by in situ growth method and its application to dye adsorption. J Solid State Chem 297:122030. https://doi.org/10.1016/j.jssc.2021.122030
16. Cimirro NFGM, Lima EC, Cunha MR et al (2022) Removal of diphenols using pine biochar Kinetics, equilibrium, thermodynamics, and mechanism of uptake. J Mole Liquids 364:119979. https://doi.org/10.1016/j.molliq.2022.119979
17. dos Reis GS, Guy M, Mathieu M et al (2022) A comparative study of chemical treatment by MgCl2, ZnSO4, ZnCl2, and KOH on physicochemical properties and acetaminophen adsorption performance of biobased porous materials from tree bark residues. Colloids Surface A: Physicochem Eng Aspects 642:128626. https://doi.org/10.1016/j.colsurfa.2022.128626
18. Guy M, Mathieu M, Anastopoulos IP et al (2022) Process Parameters Optimization, Characterization, and Application of KOH-Activated Norway Spruce Bark Graphitic Biochars for Efficient Azo Dye Adsorption. Molecules 27:456. https://doi.org/10.3390/molecules27020456
19. Yamil YL, Georgin J, dos Reis GS et al (2020) Utilization of Pacara Earpod tree (Enterolobium contortisilquum) and Ironwood (Caesalpinia leiostachya) seeds as low-cost biosorbents for removal of basic fuchsin. Environ Sci Pollut Res 27:33307–33320. https://doi.org/10.1007/s11356-020-09471-z
20. Banerjee S, Chattopadhyaya MC (2017) Adsorption characteristics for the removal of a toxic dye, tartrazine from aqueous solutions by a low cost agricultural by-product. Arab J Chem 10:S1629–S1638. https://doi.org/10.1016/j.arabjc.2013.06.005
21. Costa JAS, Paranhos CM (2019) Evaluation of rice husk ash in adsorption of Remazol Red dye from aqueous media. SN Appl Sci 1:1–8. https://doi.org/10.1007/s42452-019-0436-1
22. Tabassam N, Mutahir S, Khan MA et al (2022) Facile synthesis of cinnamic acid sensitized rice husk biochar for removal of organic dyes from wastewaters: Batch experimental and theoretical studies. Mater Chem Phys 288:126327. https://doi.org/10.1016/j.matchemphys.2022.126327
23. Bin HJ, Haque MI, Hoque M et al (2022) Efficient extraction of silica from openly burned rice husk ash as adsorbent for dye removal. J Clean Prod 380:135121. https://doi.org/10.1016/j.jclepro.2022.135121
24. Kaykioglu G, Gunes E (2016) Comparison of Acid Red 114 Dye Adsorption by Fe3O4 and Fe3O4 Impregnated Rice Husk Ash. J Nanomater. https://doi.org/10.1155/2016/6304096
25. Homagai PL, Poudel R, Poudel S, Bhattarai A (2022) Adsorption and removal of crystal violet dye from aqueous solution by modified rice husk. Heliyon 8:e09261. https://doi.org/10.1016/j.heliyon.2022.e09261
26. Quansah JO, Hlaing T, Lyonga FN et al (2020) Nascent rice husk as an adsorbent for removing cationic dyes from textile wastewater. Appl Sci (Switzerland) 10:3437. https://doi.org/10.3390/app10103437
27. Koyuncu DDE, Okur M (2021) Investigation of dye removal ability and reusability of green and sustainable silica and carbon-silica hybrid aerogels prepared from paddy waste ash. Colloids Surface A: Physicochem Eng Aspects 628:127370. https://doi.org/10.1016/j.colsurfa.2021.127370
28. Kani AN, Dovi E, Aryee AA et al (2021) Polyethylenimine modified tiger nut residue for removal of congo red from solution. Desalin Water Treat 215:209–221. https://doi.org/10.5004/dwt.2021.26765
29. Lee JH, Kim JH, Choi K et al (2018) Investigation of the mechanism of chromium removal in (3-aminopropyl)trimethoxysilane functionalized mesoporous silica. Sci Rep 8:1–11. https://doi.org/10.1038/s41598-018-29679-x
30. Cavalcante EHM, Candido ICM, de Oliveira HP et al (2022) 3-Aminopropyl-triethoxysilane-Functionalized Tannin-Rich Grape Biomass for the Adsorption of Methyl Orange Dye: Synthesis, Characterization, and the Adsorption Mechanism. ACS Omega 7:18997–19009. https://doi.org/10.1021/acsomega.2c02101
31. Maleki H, Durães L, Portugal A (2014) An overview on silica aerogels synthesis and different mechanical reinforcing strategies. J Non-Cryst Solids 385:55–74. https://doi.org/10.1016/j.jnoncrysol.2013.10.017

32. Karamikamkar S, Naguib HE, Park CB (2020) Advances in precursor system for silica-based aerogel production toward improved mechanical properties, customized morphology, and multifunctionality: A review. Adv Colloid Interface Sci 276:102101. https://doi.org/10.1016/j.cis.2020.102101
33. Halim ZAA, Yajid MAM, Hamdan H (2021) Effects of Solvent Exchange Period and Heat Treatment on Physical and Chemical Properties of Rice Husk Derived Silica Aerogels. SILICON 13:251–257. https://doi.org/10.1007/s12633-020-00421-5
34. Feng Q, Chen K, Ma D et al (2018) Synthesis of high specific surface area silica aerogel from rice husk ash via ambient pressure drying. Colloids Surf, A 539:399–406. https://doi.org/10.1016/j.colsurfa.2017.12.025
35. Guzel Kaya G, Deveci H (2020) Synergistic effects of silica aerogels/xerogels on properties of polymer composites: A review. J Ind Eng Chem 89:13–27. https://doi.org/10.1016/j.jiec.2020.05.019
36. Hasanin MS (2020) Sustainable hybrid silica extracted from rice husk with polyvinyl alcohol and nicotinic acid as multi adsorbent for textile wastewater treatment. Environ Sci Pollut Res 27:26742–26749. https://doi.org/10.1007/s11356-020-09104-5
37. Yusmaniar Y, Darwis D, Afrizal A, Annisa A (2018) Synthesis of silica of rice husk modification (3-aminopropyl) trietoxysilane for adsorption methylene blue. MATEC Web of Conferences 197:6–9. https://doi.org/10.1051/matecconf/201819709009
38. Eslek Koyuncu DD, Okur M (2022) Adsorption of Rhodamine-B from Aqueous Solution Using APTMS and GPTMS Modified Silica Sorbents. Eurasian J Med Biol Sci 2:6–13
39. Banaei A, Ebrahimi S, Vojoudi H et al (2017) Adsorption equilibrium and thermodynamics of anionic reactive dyes from aqueous solutions by using a new modified silica gel with 2,2″-(pentane-1,5-diylbis(oxy))dibenzaldehyde. Chem Eng Res Des 123:50–62. https://doi.org/10.1016/j.cherd.2017.04.032
40. Veerakumar P, Jeyapragasam T, Surabhi S et al (2019) Functionalized Mesoporous Carbon Nanostructures for Efficient Removal of Eriochrome Black-T from Aqueous Solution. J Chem Eng Data 64:1305–1321. https://doi.org/10.1021/acs.jced.8b00878
41. Donia AM, Atia AA, Al-amrani WA, El-Nahas AM (2009) Effect of structural properties of acid dyes on their adsorption behaviour from aqueous solutions by amine modified silica. J Hazard Mater 161:1544–1550. https://doi.org/10.1016/j.jhazmat.2008.05.042
42. EslekKoyuncu DD, Okur M (2021) Removal of AV 90 dye using ordered mesoporous carbon materials prepared via nanocasting of KIT-6: Adsorption isotherms, kinetics and thermodynamic analysis. Sep Purif Technol 257:117657. https://doi.org/10.1016/j.seppur.2020.117657
43. Liu G, Yang R, Li M (2010) Liquid adsorption of basic dye using silica aerogels with different textural properties. J Non-Cryst Solids 356:250–257. https://doi.org/10.1016/j.jnoncrysol.2009.11.019
44. Oguntimein GB (2015) Biosorption of dye from textile wastewater effluent onto alkali treated dried sunflower seed hull and design of a batch adsorber. J Environ Chem Eng 3:2647–2661. https://doi.org/10.1016/j.jece.2015.09.028
45. Subhan F, Aslam S, Yan Z et al (2022) Adsorption and reusability performance of hierarchically porous silica (MMZ) for the removal of MB dye from water. Inorganic Chem Commun 139:109380. https://doi.org/10.1016/j.inoche.2022.109380
46. Melnyk IV, Tomina VV, Stolyarchuk NV et al (2021) Organic dyes (acid red, fluorescein, methylene blue) and copper(II) adsorption on amino silica spherical particles with tailored surface hydrophobicity and porosity. J Mole Liquids 336:116301. https://doi.org/10.1016/j.molliq.2021.116301
47. Zhang Y, Xia K, Liu X et al (2019) Synthesis of cationic-modified silica gel and its adsorption properties for anionic dyes. J Taiwan Inst Chem Eng 102:1–8. https://doi.org/10.1016/j.jtice.2019.05.005
48. Mikhaylova M, Kim DK, Berry CC et al (2004) BSA immobilization on amine-functionalized superparamagnetic iron oxide nanoparticles. Chem Mater 16:2344–2354. https://doi.org/10.1021/cm0348904
49. Nhavene EPF, Andrade GF, Arantes Faria JAQ et al (2018) Biodegradable polymers grafted onto multifunctional mesoporous silica nanoparticles for gene delivery. ChemEngineering 2:1–16. https://doi.org/10.3390/chemengineering2020024
50. Rita S, Eti R, Tetty K (2018) Aminopropyltrimethoxysilane (APTMS) modified nano silica as heavy metal iron (Fe) adsorbents in peat water. AIP Conference Proceed 2014:. https://doi.org/10.1063/1.5054567
51. Huang X, Ke R, Dong Y (2020) Characterization and corrosion protection of nano-titanium dioxide doped BTSE-GPTMS sol–gel coating on cast Al–Si alloy. J Sol-Gel Sci Technol 94:671–680. https://doi.org/10.1007/s10971-019-05211-z
52. Reyes-Peces MV, Pérez-Moreno A, De-Los-santos DM et al (2020) Chitosan-gptms-silica hybrid mesoporous aerogels for bone tissue engineering. Polymers 12:1–24. https://doi.org/10.3390/polym12112723
53. Tran HN, Wang YF, You SJ, Chao HP (2017) Insights into the mechanism of cationic dye adsorption on activated charcoal: The importance of Π-Π interactions. Process Saf Environ Prot 107:168–180. https://doi.org/10.1016/j.psep.2017.02.010
54. Da'na E (2022) Nano-Silica Modified with Diamine for Capturing Azo Dye from Aqueous Solutions. Molecules 27:. https://doi.org/10.3390/molecules27113366
55. Liu Y, Jia H, Li C et al (2019) Efficient removal of gaseous formaldehyde by amine-modified diatomite: a combined experimental and density functional theory study. Environ Sci Pollut Res 26:25130–25141. https://doi.org/10.1007/s11356-019-05758-y
56. Qiao B, Wang TJ, Gao H, Jin Y (2015) High density silanization of nano-silica particles using γ-aminopropyltriethoxysilane (APTES). Appl Surf Sci 351:646–654. https://doi.org/10.1016/j.apsusc.2015.05.174
57. Salama A (2019) Soy protein acid hydrolysate/silica hybrid material as novel adsorbent for methylene blue. Composites Commun 12:101–105. https://doi.org/10.1016/j.coco.2019.01.002
58. Lei Y, Yang G, Huang Q et al (2022) Facile synthesis of ionic liquid modified silica nanoparticles for fast removal of anionic organic dyes with extremely high adsorption capacity. J Mole Liquids 347:117966. https://doi.org/10.1016/j.molliq.2021.117966
59. Chen M, Shen Y, Xu L et al (2021) Highly efficient and rapid adsorption of methylene blue dye onto vinyl hybrid silica nanocross-linked nanocomposite hydrogel. Colloids Surface A: Physicochem Eng Aspects 613:126050. https://doi.org/10.1016/j.colsurfa.2020.126050
60. Mahmoodi NM, Mokhtari-Shourijeh Z, Langari S et al (2021) Silica aerogel/polyacrylonitrile/polyvinylidene fluoride nanofiber and its ability for treatment of colored wastewater. J Mole Structure 1227:129418. https://doi.org/10.1016/j.molstruc.2020.129418